Am J Transl Res 2019;11(11):6790-6811
www.ajtr.org /ISSN:1943-8141/AJTR0099680

Original Article

Unraveling the action mechanism of *polygonum cuspidatum* by a network pharmacology approach

Boyu Pan[1], Xiaona Shi[3], Tingting Ding[2], Liren Liu[1]

Departments of [1]Gastrointestinal Cancer Biology, [2]Pathology, Tianjin Medical University Cancer Institute and Hospital, National Clinical Research Center for Cancer, Key Laboratory of Cancer Prevention and Therapy, Tianjin's Clinical Research Center for Cancer, Tianjin 300060, China; [3]Tianjin International Joint Academy of Biotechnology and Medicine Analytical Testing Center, Tianjin 300457, China

Received July 15, 2019; Accepted November 2, 2019; Epub November 15, 2019; Published November 30, 2019

Abstract: As a popular Chinese herbal medicine (CHM), *polygonum cuspidatum* is widely used to treat various diseases in China. However, its biological function and action mechanism have yet to be systematically explored. In the present study, we first identified 14 potential active ingredients of *polygonum cuspidatum* using the TCMSP server and then conducted an *in silico* target prediction for these ingredients using PharmMapper. The subsequent KEGG pathway enrichment analysis of the 57 identified potential targets revealed that they were closely associated with cancer and gynecological disorders. Furthermore, a protein-protein interaction network of these targets was constructed using STRING and Cytoscape, through which 11 core targets were excavated according to degree, a key topological parameter. Meanwhile, we developed a novel formula, in which the "R value" is determined by average shortest path length and closeness centrality, two other key topological parameters, to evaluate the reliability of these predicted core targets. Intriguingly, among the top 10 core targets excavated using this new formula, 7 overlapped with the former 11 core targets, showing a good consistency in these core targets between the different prediction algorithms. Next, 7 ingredients were identified/validated from the crude extract of *polygonum cuspidatum* using UPLC-MS/MS. Noteworthy, 6 potential targets predicted for these 7 ingredients overlapped with the 7 core targets excavated from the previous *in silico* analyses. Further molecular docking and druggability analyses suggested that polydatin may play a pivotal role in manifesting the therapeutic effects of *polygonum cuspidatum*. Finally, we carried out a series of cell functional assays, which validated the anti-proliferative effects of *polygonum cuspidatum* on gynecological cancer cells, thus demonstrating our network pharmacology approach is reliable and powerful enough to guide the CHM mechanism study.

Keywords: *Polygonum cuspidatum* (Hu Zhang), Chinese herb medicine, network pharmacology, UPLC-MS/MS, polydatin

Introduction

From ancient times to the present, Chinese herbal medicine (CHM) has been applied to prevent and treat various diseases in China. Nowadays, owing to its distinct therapeutic effects, CHM has been attracting more and more attention worldwide [1-3]. *Polygonum cuspidatum* (Hu Zhang), widely distributed in southern China, is a popular CHM with a wide range of pharmacological and biological activities. To date, > 100 prescriptions containing this plant have been used to treat a large variety of diseases, such as infection, inflammation, skin burns and hyperlipemia [4, 5]. However, current knowledge about the medicinal characteristics of *polygonum cuspidatum* is incomplete, and a deeper understanding of its system-level action mechanism is required.

Composed of multiple ingredients, CHM has holistic and synergistic effects on complicated diseases. However, the action mechanism study of CHM is hindered by the complicated interactions among its "multi-ingredients" and the affected "multi-targets". Network pharmacology has been lately applied to CHM research and is considered to be a promising approach to overcoming the above obstacle. Based on the network of "drug-target-disease-pathway"

interactions, network pharmacology can reveal the synergistic effects on human systems by complex CHM. Meanwhile, with the recent advances in computational methods, bioinformatics has been used for the target prediction for CHM, which has significantly promoted the mechanism study of CHM [6, 7]. Thus, in conjunction with bioinformatics, network pharmacology is now a powerful tool for untangling the disease-disease, disease-target protein, target protein-drug and drug-drug interactions among multi-ingredient CHM and complicated diseases [8-11].

Herein, in order to unravel the action mechanism of *polygonum cuspidatum,* we first screened active ingredients in *polygonum cuspidatum* using the TCMSP server and a literature search, followed with ingredient-target prediction by reverse docking analysis. GO functional and KEGG pathway enrichment analyses of the potential protein targets were then performed and the following constructed drug-target-pathway network revealed a great diversity of biological functions of *polygonum cuspidatum*. Thus, by taking advantage of the recent advances in network pharmacology and bioinformatics, we provided an overview on the action mechanism of active ingredients in *polygonum cuspidatum*, achieving a comprehensive understanding of its holistic therapeutic effect on specific diseases.

Materials and methods

Cell culture and reagents

Human breast cancer MDA-MB-231 cells and ovarian cancer SKOV-3 cells were obtained from the China Infrastructure of Cell Line Resources (School of Basic Medicine Peking Union Medical College, China) and were maintained in RPMI-1640 medium supplemented with 10% (v/v) FBS and 100 U/ml streptomycin/penicillin in the humidified atmosphere of 5% CO_2 at 37°C. RPMI-1640 medium were purchased from GIBCO (USA). Fetal bovine serum (FBS) was purchased from ThermoFisher (USA). Cell Counting Kit-8 (CCK-8) reagent was bought from Dojindo (Japan). Annexin-V FITC apoptosis detection kit (#556547) was purchased from BD Biosciences Pharmingen (USA). The standard of *polygonum cuspidatum* was obtained from China National Institutes for Food and Drug Control.

Screening of active ingredients and relative target prediction

The value of oral bioavailability (OB) was evaluated by the OBioavail 1.1 model in the TCMSP database (http://ibts.hkbu.edu.hk/LSPtcmsp.php). Meanwhile, drug-likeness (DL) was analyzed using a model from the TCMSP database, which was constructed on account of the molecular descriptors and Tanimoto coefficient [12, 13]. The parameters for the selection of active ingredients were set as follows: OB ≥ 30% and DL ≥ 0.18. The Tripos mol2 type files of the selected active ingredients were searched using the TCMSP database. Next, the potential protein targets were predicted by importing each component file with mol2 format into the PharmMapper reverse docking database in May 2018. By normalized fit score, the top 10 high-matching targets for each of the active ingredients were selected and the overlapped ones were excluded. The selected targets were then searched in the Uniprot database to identify their human-related protein target codes.

GO and KEGG enrichment analysis, and systematic network construction

Functional enrichment of GO was performed using OmicShare tools, a free online platform for data analysis (http://www.omicshare.com/tools) [14]. Meanwhile, potential protein targets were uploaded to the DAVID Bioinformatics Resources 6.8 server (https://david.ncifcrf.gov/summary.jsp) for KEGG pathway enrichment analysis. In order to obtain a deeper understanding of the complex relationships among drug, protein targets and pathways, a systematic network was constructed using Cytoscape 3.2.1. In GO and KEGG analysis, $P < 0.05$ was defined as significantly enriched.

PPI network construction and excavation of core genes

All potential protein targets were uploaded to the STRING database (http://string-db.org/) to analyze their interactions. Comprehensive information on the interactions of these protein targets was downloaded from STRING, and the interactions with a combined score of > 0.4 were selected for the construction of the PPI network using Cytoscape 3.2.1. The core genes from the PPI network were excavat-

Table 1. Primer sequences of mRNA structural components used in q-PCR

Components	Position	Sequence
EGFR	Forward	AGGCACGAGTAACAAGCTCAC
	Reverse	ATGAGGACATAACCAGCCACC
CASP3	Forward	CATGGAAGCGAATCAATGGACT
	Reverse	CTGTACCAGACCGAGATGTCA
ALB	Forward	TCGGCTTATTCCAGGGGTGT
	Reverse	AAGGCAATCAACACCAAGGCT
MAPK14	Forward	GCACTGAAGAAGCTGTCGAG
	Reverse	GAACGTGGTCATCGGTAAGC
F2	Forward	CTGAGGGTCTGGGTACGAACT
	Reverse	TGGGTAGCGACTCCTCCATAG
ESR1	Forward	GGGAAGTATGGCTATGGAATCTG
	Reverse	TGGCTGGACACATATAGTCGTT
GAPDH	Forward	TGCACCACCAACTGCTTAGC
	Reverse	GGCATGGACTGTGGTCATGAG

ed using Degree, a key topological parameter, with the cut-off criteria of DC scores of ≥ 10. Furthermore, the average shortest path length and closeness centrality, another two topological parameters, were calculated by NetworkAnalyzer [15]. R-value was used to determine the ranks of the targets of *polygonum cuspidatum* using the following formula:

$$R = \frac{X_a - X_a(\min)}{X_a(\max) - X_a(\min)} \times 50\% + \frac{\frac{1}{X_b} - \frac{1}{X_b}(\min)}{\frac{1}{X_b}(\max) - \frac{1}{X_b}(\min)} \times 50\%$$

This formula used the idea of normalization, where x_a was the average shortest path length, x_b was the closeness centrality, and R was an indicator to evaluate the importance of a target.

Cellular functional assays

The cell viability was assessed by the CCK-8 assay, in which 10 μl of CCK-8 was added to each well, and the cells were incubated for an additional two hours before the absorbance value was measured at a wavelength of 450 nm using an automated microplate reader. Apoptosis detection and Western Blot assay were performed according to the manufacturer's instructions.

Liquid chromatography, mass spectrometric conditions and sample extraction preparation

Liquid chromatographic separation and mass spectrometric detection were performed using Waters Quattro Premier XE/Acquity UPLC system coupled to a tandem quadrupole mass spectrometer (Waters Corporation, Milford, MA, USA). Lab solutions LCMS software (Masslynx V4.1) was used to control the instruments and process the data. This instrument was equipped with both ESI and APCI sources. Chromatographic separation was performed using an Agilent Eclipse PlusC18 column (100 × 4.6 mm, 3.5 μm) at a flow rate of 0.4 ml/min in ESI source. The isocratic mobile phase consisted of methanol and 0.01% formic acid with gradient elution; run times were from 0-20 min with 10-90% B, 20-22 min with 90% B, 22-25 min with 90-10% B and 25-30 min with 10% B. The mass spectrometer operating parameters were optimized as follows: Interface voltage, 3.2 kV; desolvation temperature, 450°C; source temperature, 120°C. Analyst software version Masslynx V4.1 was used to control all parameters of liquid chromatography and mass spectrometry (MS).

Total RNA extraction and quantitative real-time PCR

Total RNA from breast cancer and ovarian cancer cells were extracted using the TRIzol reagent. The total RNA was quantified using Nano-drop 1000 (Thermo Fisher Scientific, USA). Two microgram of the total RNA from each sample was used for cDNA synthesis with PrimeScript RT Master Mix reagent according to the manufacturer's protocol. By using the specific primer pairs (**Table 1**) and SYBR GREEN Premix reagent, qRT-PCR was performed on the QuantStudio 5 real-time PCR system (Thermo Fisher Scientific, USA). Expression data were normalized to the geometric mean of the housekeeping GAPDH gene to control the variability in mRNA expression levels.

Systemsdock analysis

SystemsDock online tools were first utilized to check the docking efficiency between the 6 core genes and 7 key ingredients. The PDB ID of 6 core targets and Tripos mol2 type files of these ingredients was inputted simultaneously into the system for further analysis. Next polydatin and CASP3 (PDB ID: 4QUJ) were redocked by Autodock software, and the top 30 docking conformations were extracted and selected as the best phase of docking energy for further analysis.

Statistical analysis

All data were analyzed using SPSS17.0 software (SPSS, Inc., Chicago, IL, USA). Results are represented as the mean ± standard deviation. Student's t-test is used for comparisons between different groups. $P < 0.05$ was considered to indicate a statistically significant difference.

Results

Selection of the potential active ingredients in polygonum cuspidatum and prediction of their potential protein targets

First, using the TCMSP server, a unique systems-level pharmacology platform for CHM, we calculated ADME-related characteristics for all ingredients of polygonum cuspidatum. The specific pharmacokinetic properties of these ingredients undergoing evaluation included OB, DL, CaCo-2 permeability, blood-brain barrier permeability and Lipinski's rule of five (MW, AlogP, TPSA, Hdon and Hacc). Since OB and DL represent the most important pharmacokinetic properties, the selection parameter for the active ingredients was set as follows: OB ≥ 30% and DL ≥ 0.18 [12, 13, 16]. Based on this threshold, we obtained 9/62 active ingredients of *polygonum cuspidatum*, namely physovenine, rhein, catechin, quercetin, beta-sitosterol, picralinal, physciondiglucoside, torachrysone-8-O-beta-D-(6'-oxayl)-glucoside and luteolin. Another 5 key active ingredients, namely emodin, chrysophanol, resveratrol, polydatin and apigenin were also included for further analysis referring to previous studies [17, 18], although they did not meet all aforementioned criteria. We therefore finally screened out 14 active ingredients of *polygonum cuspidatum* for further protein target prediction. The structure and ADME-related characteristics of the above ingredients are shown in **Figure 1** and **Table 2**, respectively.

Next, we predicted the potential targets for each of these 14 ingredients using the PharmMapper reverse docking database. By normalized fit score, the top 10 high-matching targets for each of the 14 ingredients were selected for further analysis. After ruling out the ones that overlapped, we finally obtained a total of 57 potential protein targets for these 14 ingredients (**Table 3**).

Enrichment analysis and systematic network construction for the putative protein targets

To explore the potential action mechanism of *polygonum cuspidatum,* GO functional and KEGG pathway enrichment analyses were performed for these 57 targets using OmicShare online tools and DAVID Bioinformatics Resources 6.8, respectively. Based on $P < 0.05$, the top 5 terms associated with gene counts in biological process were metabolic process, cellular process, single-organism process, response to stimulus and biological regulation. The top 5 terms associated with gene counts in cellular component were cell, cell part, organelle, extracellular region, and membrane. The top 5 terms associated with gene counts in molecular function were binding, catalytic activity, molecular transducer activity, signal transducer activity, and molecular function regulator. These predictive results showed a great diversity in biological functions of *polygonum cuspidatum* (**Figure 2A**). Based on $P < 0.05$, the top 8 KEGG pathways associated with gene counts were pathways in cancer, tuberculosis, mitogen-activated protein kinase 1 (MAPK) signaling pathway, prolactin signaling pathway, progesterone-mediated oocyte-maturation pathway, tumor necrosis factor (TNF) signaling pathway, pathways in hepatitis B and viral carcinogenesis. Of note, we found that the above pathways were closely associated with cancer and gynecological disorders. In fact, previous studies have shown that certain active ingredients in *polygonum cuspidatum*, such as polydatin, resveratrol and emodin, exhibit potential therapeutic effects against these diseases [4, 19-21] (See **Table 4** and **Figure 2B** for details). Further, to provide a systematic overview of the involved signaling pathways and the potential molecular action mechanism of *polygonum cuspidatum*, we constructed a comprehensive network composed of drug, protein targets and pathways using Cytoscape 3.2.1, based on the results of the above target prediction and pathway enrichment analysis (**Figure 2C**). The red diamond, orange oval and green rectangle represent 14 active ingredients, protein targets and associated pathways, respectively.

PPI network construction and core gene enrichment analysis

PPI modulation has been attracting increasing attention, and the properties of PPI, such as all

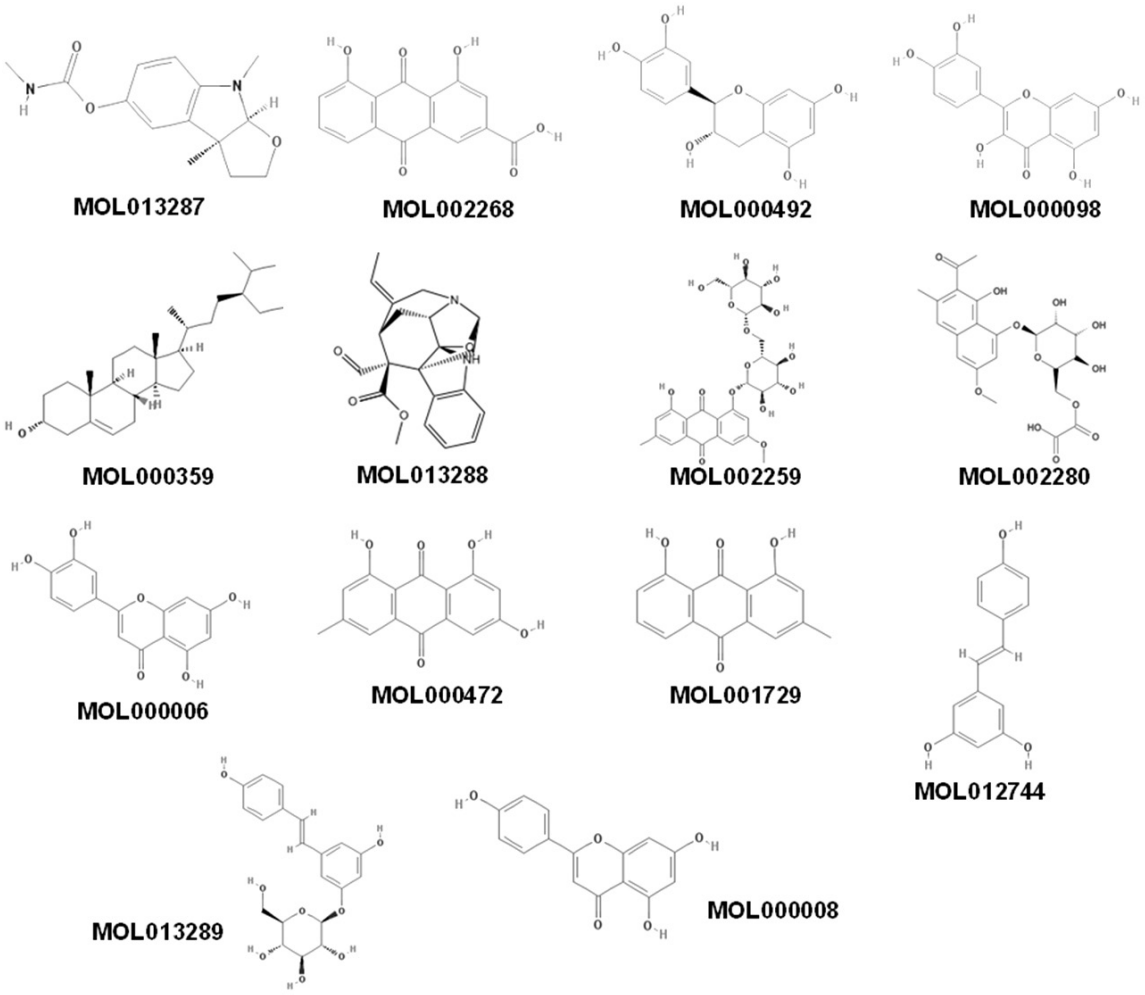

Figure 1. Chemical structure of fourteen active ingredients of polygonum cuspidatum downloaded from the TCMSP database. These fourteen active ingredients are: physovenine (MOL013287), rhein (MOL002268), catechin (MOL000492), quercetin (MOL000098), beta-sitosterol (MOL000359), picralinal (MOL013288), physciondiglucoside (MOL002259), torachrysone-8-O-beta-D-(6'-oxayl)-glucoside (MOL002280), luteolin (MOL000006), emodin (MOL000472), chrysophanol (MOL001729), resveratrol (MOL012744), polydatin (MOL013289) and apigenin (MOL000008).

osteric sites and hotspots, have been considered by various modern drug-design strategies. We therefore visualized the potential interactions between the 57 protein targets by constructing a PPI network using degree, a key topological parameter, with 'DC' scores of ≥ 10 as the cut-off criteria. In total, 50 nodes and 176 edges were generated in this network (**Figure 3**). The warm color nodes represented a higher degree of core, compared to the cold color nodes within the network. According to the 'DC' levels, the 11 core nodes were: Serum albumin (ALB; degree, 34), epidermal growth factor receptor (EGFR; degree, 22), ESR1 (degree, 21), MAPK1 (degree, 19), prothrombin (F2; degree, 17), caspase-3 (CASP3; degree, 17), MAPK8 (degree, 16), MAPK14 (degree, 16), progesterone receptor (degree, 14), androgen receptor (degree, 12) and plasminogen (degree, 12) (**Table 5**).

To evaluate the reliability of these core targets, we conducted another core target prediction using a novel formula, which takes the average shortest path length and closeness centrality as the key topological parameters. According to the R-value calculated by this formula, the top 10 core targets of *polygonum cuspidatum*are presented in **Table 6**. Of note, 7 core targets, namely EGFR, MAPK1, CASP3, ALB, MAPK14, F2 and ESR1, were overlapping in both topological analyses, demonstrating a good consistency among the different prediction algorithms.

Table 2. Pharmacological and molecular parameters of *Polygonum cuspidatum*

MOL_ID	Name	MW	AlogP	Hdon	Hacc	OB (%)	CaCo-2	BBB	DL	TPSA	RBN
MOL013287	Physovenine	262.34	2.08	1	5	106.21	0.51	0.20	0.19	50.80	2
MOL002268	Rhein	284.23	1.88	3	6	47.07	-0.20	-0.99	0.28	111.90	1
MOL000492	Catechin	290.29	1.92	5	6	54.83	-0.03	-0.73	0.24	110.38	1
MOL000098	Quercetin	302.25	1.50	5	7	46.43	0.05	-0.77	0.28	131.36	1
MOL000359	Beta-sitosterol	414.79	8.08	1	1	36.91	1.32	0.87	0.75	20.23	6
MOL013288	Picralinal	366.45	1.80	1	6	58.01	0.23	-0.21	0.75	67.87	3
MOL002259	Physciondiglucoside	608.60	-0.91	8	15	41.65	-2.64	-3.43	0.63	242.13	7
MOL002280	Torachrysone-8-O-beta-D-(6'-oxayl)-glucoside	480.46	0.64	5	12	43.02	-1.23	-1.84	0.74	189.28	8
MOL000006	Luteolin	286.25	2.07	4	6	36.16	0.19	-0.84	0.25	111.13	1
MOL000472	Emodin	270.25	2.49	3	5	24.40	0.22	-0.66	0.24	94.83	0
MOL001729	Chrysophanol	254.25	2.76	2	4	18.64	0.62	-0.20	0.21	74.60	0
MOL012744	Resveratrol	228.26	3.01	3	3	19.07	0.80	-0.01	0.11	60.69	2
MOL013289	Polydatin	390.42	1.11	6	8	21.44	-0.90	-1.81	0.50	139.84	5
MOL000008	Apigenin	270.25	2.33	3	5	23.06	0.43	-0.61	0.21	90.90	1

Table 3. The potential protein targets of 14 active ingredients in *Polygonum cuspidatum*

No.	Compound	Protein code	Protein name	Normalized Fit Score
1	physovenine	P12643	BMP2_HUMAN	1
2	physovenine	P00918	CAH2_HUMAN	0.9951
3	physovenine	P09211	GSTP1_HUMAN	0.9721
4	physovenine	P20701	ITAL_HUMAN	0.9492
5	physovenine	P62937	PPIA_HUMAN	0.947
6	physovenine	P06276	CHLE_HUMAN	0.9338
7	physovenine	P52895	AK1C2_HUMAN	0.9275
8	physovenine	P15121	ALDR_HUMAN	0.9
9	physovenine	Q8NBQ5	DHB11_HUMAN	0.8863
10	physovenine	P23946	CMA1_HUMAN	0.8543
11	rhein	P00751	CFAB_HUMAN	0.9897
12	rhein	P45983	MK08_HUMAN	0.9685
13	rhein	P53779	MK10_HUMAN	0.9645
14	rhein	Q16539	MK14_HUMAN	0.9632
15	rhein	P08254	MMP3_HUMAN	0.9579
16	rhein	P62937	PPIA_HUMAN	0.9431
17	rhein	P11511	CP19A_HUMAN	0.9312
18	rhein	O14965	AURKA_HUMAN	0.9268
19	rhein	O14757	CHK1_HUMAN	0.9137
20	rhein	Q8NBQ5	DHB11_HUMAN	0.9066
21	(+)-catechin	P10275	ANDR_HUMAN	0.9896
22	(+)-catechin	P00751	CFAB_HUMAN	0.9833
23	(+)-catechin	P08631	HCK_HUMAN	0.9827
24	(+)-catechin	P11309	PIM1_HUMAN	0.982
25	(+)-catechin	P11511	CP19A_HUMAN	0.98
26	(+)-catechin	P02766	TTHY_HUMAN	0.9791
27	(+)-catechin	P00734	THRB_HUMAN	0.9761
28	(+)-catechin	P56817	BACE1_HUMAN	0.9732
29	(+)-catechin	P03372	ESR1_HUMAN	0.9552
30	(+)-catechin	P00390	GSHR_HUMAN	0.9544
31	quercetin	P11309	PIM1_HUMAN	0.989
32	quercetin	P08631	HCK_HUMAN	0.9854
33	quercetin	P03372	ESR1_HUMAN	0.9615
34	quercetin	P06276	CHLE_HUMAN	0.9492
35	quercetin	P00734	THRB_HUMAN	0.9491
36	quercetin	P06401	PRGR_HUMAN	0.9356
37	quercetin	P00533	EGFR_HUMAN	0.9333
38	quercetin	P02766	TTHY_HUMAN	0.9264
39	quercetin	P00918	CAH2_HUMAN	0.9077
40	quercetin	P04062	GLCM_HUMAN	0.8908
41	beta-sitosterol	P52895	AK1C2_HUMAN	0.9987
42	beta-sitosterol	P28482	MK01_HUMAN	0.9959
43	beta-sitosterol	P49137	MAPK2_HUMAN	0.9954
44	beta-sitosterol	P11309	PIM1_HUMAN	0.9921
45	beta-sitosterol	P12643	BMP2_HUMAN	0.9914
46	beta-sitosterol	P00918	CAH2_HUMAN	0.9893
47	beta-sitosterol	P10828	THB_HUMAN	0.9845

48	beta-sitosterol	P02768	ALBU_HUMAN	0.9838
49	beta-sitosterol	P27338	AOFB_HUMAN	0.9779
50	beta-sitosterol	P08842	STS_HUMAN	0.9734
51	picralinal	P08254	MMP3_HUMAN	0.9695
52	picralinal	P23141	EST1_HUMAN	0.9578
53	picralinal	Q15078	CD5R1_HUMAN	0.8947
54	picralinal	P53779	MK10_HUMAN	0.8889
55	picralinal	P06276	CHLE_HUMAN	0.8705
56	picralinal	P26196	DDX6_HUMAN	0.8705
57	picralinal	P00747	PLMN_HUMAN	0.8672
58	picralinal	P45983	MK08_HUMAN	0.8601
59	picralinal	P55055	NR1H2_HUMAN	0.8567
60	picralinal	P00918	CAH2_HUMAN	0.8265
61	physciondiglucoside	P04062	GLCM_HUMAN	0.9965
62	physciondiglucoside	Q9BW91	NUDT9_HUMAN	0.9911
63	physciondiglucoside	Q12884	SEPR_HUMAN	0.9909
64	physciondiglucoside	P17342	ANPRC_HUMAN	0.9886
65	physciondiglucoside	P12643	BMP2_HUMAN	0.9881
66	physciondiglucoside	P08631	HCK_HUMAN	0.9771
67	physciondiglucoside	Q07343	PDE4B_HUMAN	0.9762
68	physciondiglucoside	P11309	PIM1_HUMAN	0.974
69	physciondiglucoside	P08254	MMP3_HUMAN	0.9713
70	physciondiglucoside	P00915	CAH1_HUMAN	0.9709
71	torachrysone-8-O-beta-D-(6'-oxayl)-glucoside	P07339	CATD_HUMAN	0.986
72	torachrysone-8-O-beta-D-(6'-oxayl)-glucoside	P53582	MAP11_HUMAN	0.9859
73	torachrysone-8-O-beta-D-(6'-oxayl)-glucoside	P09211	GSTP1_HUMAN	0.9845
74	torachrysone-8-O-beta-D-(6'-oxayl)-glucoside	Q12884	SEPR_HUMAN	0.9818
75	torachrysone-8-O-beta-D-(6'-oxayl)-glucoside	P09012	SNRPA_HUMAN	0.9816
76	torachrysone-8-O-beta-D-(6'-oxayl)-glucoside	P25774	CATS_HUMAN	0.9809
77	torachrysone-8-O-beta-D-(6'-oxayl)-glucoside	P26196	DDX6_HUMAN	0.9808
78	torachrysone-8-O-beta-D-(6'-oxayl)-glucoside	P04062	GLCM_HUMAN	0.9802
79	torachrysone-8-O-beta-D-(6'-oxayl)-glucoside	P06276	CHLE_HUMAN	0.9775
80	torachrysone-8-O-beta-D-(6'-oxayl)-glucoside	P62937	PPIA_HUMAN	0.9774
81	luteolin	P08631	HCK_HUMAN	0.9897
82	luteolin	P03372	ESR1_HUMAN	0.9684
83	luteolin	P06276	CHLE_HUMAN	0.9571
84	luteolin	P00734	THRB_HUMAN	0.9418
85	luteolin	Q12884	SEPR_HUMAN	0.9349
86	luteolin	P02766	TTHY_HUMAN	0.9242
87	luteolin	P00918	CAH2_HUMAN	0.9239
88	luteolin	P11309	PIM1_HUMAN	0.8977
89	luteolin	Q00534	CDK6_HUMAN	0.8816
90	luteolin	P00533	EGFR_HUMAN	0.8601
91	emodin	P45983	MK08_HUMAN	0.974
92	emodin	P02652	APOA2_HUMAN	0.9728
93	emodin	P08842	STS_HUMAN	0.9697
94	emodin	P53779	MK10_HUMAN	0.9658
95	emodin	Q15078	CD5R1_HUMAN	0.9655
96	emodin	P06276	CHLE_HUMAN	0.9651

97	emodin	P03372	ESR1_HUMAN	0.9642
98	emodin	P00918	CAH2_HUMAN	0.9526
99	emodin	P02768	ALBU_HUMAN	0.9517
100	emodin	P00915	CAH1_HUMAN	0.9411
101	chrysophanol	P08254	MMP3_HUMAN	0.9971
102	chrysophanol	P56817	BACE1_HUMAN	0.9635
103	chrysophanol	P00751	CFAB_HUMAN	0.961
104	chrysophanol	P45983	MK08_HUMAN	0.9487
105	chrysophanol	P06276	CHLE_HUMAN	0.9482
106	chrysophanol	P53779	MK10_HUMAN	0.9449
107	chrysophanol	P62937	PPIA_HUMAN	0.9429
108	chrysophanol	P00734	THRB_HUMAN	0.9402
109	chrysophanol	Q16539	MK14_HUMAN	0.9333
110	chrysophanol	P03372	ESR1_HUMAN	0.9302
111	resveratrol	P08631	HCK_HUMAN	0.9869
112	resveratrol	P02652	APOA2_HUMAN	0.9784
113	resveratrol	P03372	ESR1_HUMAN	0.9764
114	resveratrol	P08842	STS_HUMAN	0.9671
115	resveratrol	P56817	BACE1_HUMAN	0.9609
116	resveratrol	P11309	PIM1_HUMAN	0.9573
117	resveratrol	P00918	CAH2_HUMAN	0.9552
118	resveratrol	P02768	ALBU_HUMAN	0.9518
119	resveratrol	P20248	CCNA2_HUMAN	0.8837
120	resveratrol	P02766	TTHY_HUMAN	0.8764
121	polydatin	Q9BW91	NUDT9_HUMAN	0.991
122	polydatin	P54760	EPHB4_HUMAN	0.9847
123	polydatin	P02652	APOA2_HUMAN	0.9802
124	polydatin	P08631	HCK_HUMAN	0.9783
125	polydatin	Q13126	MTAP_HUMAN	0.9767
126	polydatin	P03372	ESR1_HUMAN	0.9762
127	polydatin	Q9NP99	TREM1_HUMAN	0.9762
128	polydatin	P04062	GLCM_HUMAN	0.976
129	polydatin	P09211	GSTP1_HUMAN	0.9739
130	polydatin	P42574	CASP3_HUMAN	0.9716
131	apigenin	P08631	HCK_HUMAN	0.9931
132	apigenin	P03372	ESR1_HUMAN	0.981
133	apigenin	P11309	PIM1_HUMAN	0.9718
134	apigenin	P06276	CHLE_HUMAN	0.9705
135	apigenin	P04062	GLCM_HUMAN	0.9521
136	apigenin	Q00534	CDK6_HUMAN	0.9
137	apigenin	P02766	TTHY_HUMAN	0.8903
138	apigenin	P00918	CAH2_HUMAN	0.8389
139	apigenin	P27338	AOFB_HUMAN	0.7953
140	apigenin	Q92731	ESR2_HUMAN	0.773

Identification of the key ingredients in polygonum cuspidatum by UPLC-MS/MS and prediction of their potential drug targets

To validate the 14 key ingredients previously selected based on the ADME-related characteristics and literature search, we next set out to identify the ingredients from the crude extract of *polygonum cuspidatum* using the UPLC-MS/MS method. Seven main ingredients of *polygonum cuspidatum*were identified, including resveratrol (t_R: 11.89 min), emodin (t_R: 23.70 min),

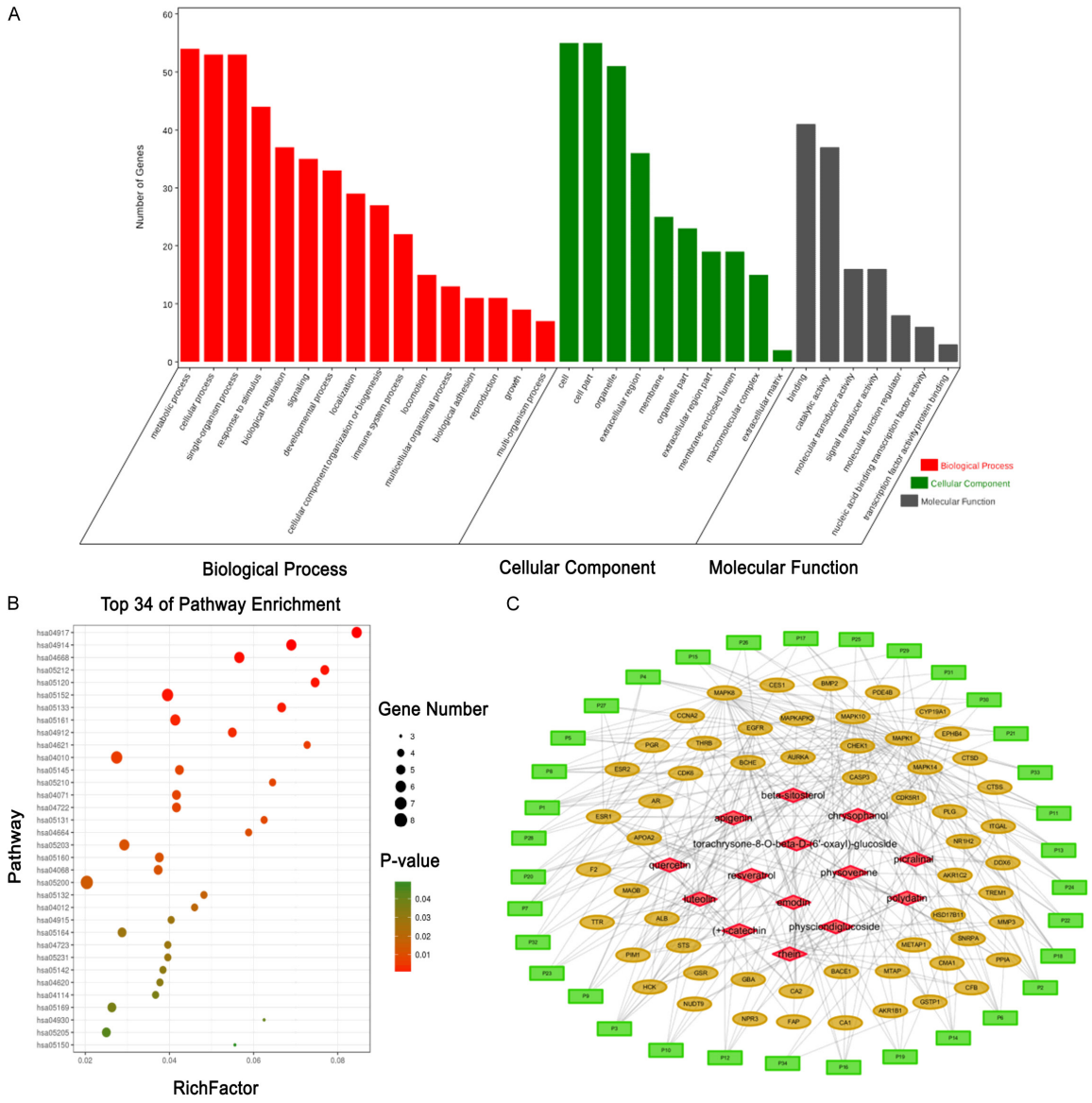

Figure 2. GO and KEGG enrichment analyses, and systematic network construction. A. GO enrichment analysis map of *polygonum cuspidatum* potential drug targets by Omicshare tools, containingBiological Process (BP), Cellular Component (CC) and Molecular Function (MF). B. KEGG enrichment analysis map of *polygonum cuspidatum* potential drug targets by DAVID Bioinformatics Resources 6.8. The size of the dots indicated the number of enriched genes, and the color of the dots represented the degree of significance based on the *p*-value. C. Drug-target-pathway network construction by Cytoscape 3.2.1. Red diamond: fourteen active ingredients in *polygonum cuspidatum*; Orange oval: protein targets; Green rectangle: pathways.

apigenin (t_R: 17.52 min), rhein (t_R: 19.54 min), catechin (t_R: 10.37 min), quercetin (t_R: 17.08 min) and polydatin (t_R: 11.73 min) (**Figure 4A-D**; see **Table 7** for details).

The potential drug targets for each of these 7 ingredients were then predicted using PharmMapper, and a total of 38 potential protein targets for these 7 ingredients were finally obtained. Interestingly, among these targets, 6 overlapped with the 7 core targets excavated from the previous topological analyses, including EGFR, CASP3, ALB, MAPK14, F2 and ESR1, demonstrating that the network pharmacology approach is a reliable and powerful tool for the study of the CHM mechanism (**Figure 4E**).

Subsequent pathway enrichment analysis revealed that these 6 core genes were mainly enriched in proteoglycans in cancer and the MAPK signaling pathway (**Figure 4F**). Meanwhile, other pathways, such as the prolactin, estrogen and TNF signaling pathways, as well as pathways in cancer, were also enriched in

Table 4. The potential pathways targeted by 14 active ingredients in *Polygonum cuspidatum*

No. of pathway	Pathway name	Gene count	*P*-Value
P1	hsa05200: Pathways in cancer	8	0.014268208
P2	hsa05152: Tuberculosis	7	0.001037853
P3	hsa04010: MAPK signaling pathway	7	0.006458276
P4	hsa04917: Prolactin signaling pathway	6	9.82E-05
P5	hsa04914: Progesterone-mediated oocyte maturation	6	2.57E-04
P6	hsa04668: TNF signaling pathway	6	6.42E-04
P7	hsa05161: Hepatitis B	6	0.002604716
P8	hsa05203: Viral carcinogenesis	6	0.011172984
P9	hsa05212: Pancreatic cancer	5	8.65E-04
P10	hsa05120: Epithelial cell signaling in Helicobacter pylori infection	5	9.70E-04
P11	hsa05133: Pertussis	5	0.001479731
P12	hsa04912: GnRH signaling pathway	5	0.003011311
P13	hsa05145: Toxoplasmosis	5	0.007589309
P14	hsa04071: Sphingolipid signaling pathway	5	0.008046143
P15	hsa04722: Neurotrophin signaling pathway	5	0.008046143
P16	hsa05160: Hepatitis C	5	0.011461535
P17	hsa04068: FoxO signaling pathway	5	0.01175749
P18	hsa05164: Influenza A	5	0.027878996
P19	hsa05169: Epstein-Barr virus infection	5	0.036826594
P20	hsa05205: Proteoglycans in cancer	5	0.043176273
P21	hsa04621: NOD-like receptor signaling pathway	4	0.005687485
P22	hsa05210: Colorectal cancer	4	0.007937757
P23	hsa05131: Shigellosis	4	0.008664099
P24	hsa04664: Fc epsilon RI signaling pathway	4	0.010230966
P25	hsa05132: Salmonella infection	4	0.017504498
P26	hsa04012: ErbB signaling pathway	4	0.019825453
P27	hsa04915: Estrogen signaling pathway	4	0.02776564
P28	hsa05231: Choline metabolism in cancer	4	0.029231619
P29	hsa04723: Retrograde endocannabinoid signaling	4	0.029231619
P30	hsa05142: Chagas disease (American trypanosomiasis)	4	0.031506722
P31	hsa04620: Toll-like receptor signaling pathway	4	0.033074068
P32	hsa04114: Oocyte meiosis	4	0.035500697
P33	hsa04930: Type II diabetes mellitus	3	0.040291089
P34	hsa05150: Staphylococcus aureus infection	3	0.049852736

this analysis, which was consistent with the results of the aforementioned pathway enrichment analysis for the 57 putative targets. These results suggested that these core genes are closely correlated with cancer and gynecological diseases, which was also in line with previous reports [22, 23].

Polygonum cuspidatum decreased the cell viability and induced the apoptosis of MDA-MB-231 and SKOV-3 cells

To validate the potential therapeutic effects of *polygonum cuspidatum* on cancer and gynecological disorders, we next carried out a series of cell functional assays, using human breast cancer MDA-MB-231 and ovarian cancer SKOV-3 cells as the experimental models of these diseases. The results of the CCK-8 assay revealed that the viability of both cells was significantly inhibited by *polygonum cuspidatum* in a dose and time dependent manner (**Figure 5A**, **5B**). After treating these cells for 24 h, IC50 analysis indicated that *polygonum cuspidatum* exerted its 50% inhibitory effect on MDA-MB-231 cells at 31.18 ± 1.95 μg/ml and SKOV-3 cells at 28.12 ± 1.07 μg/ml, respectively. Based on the above IC50 values,

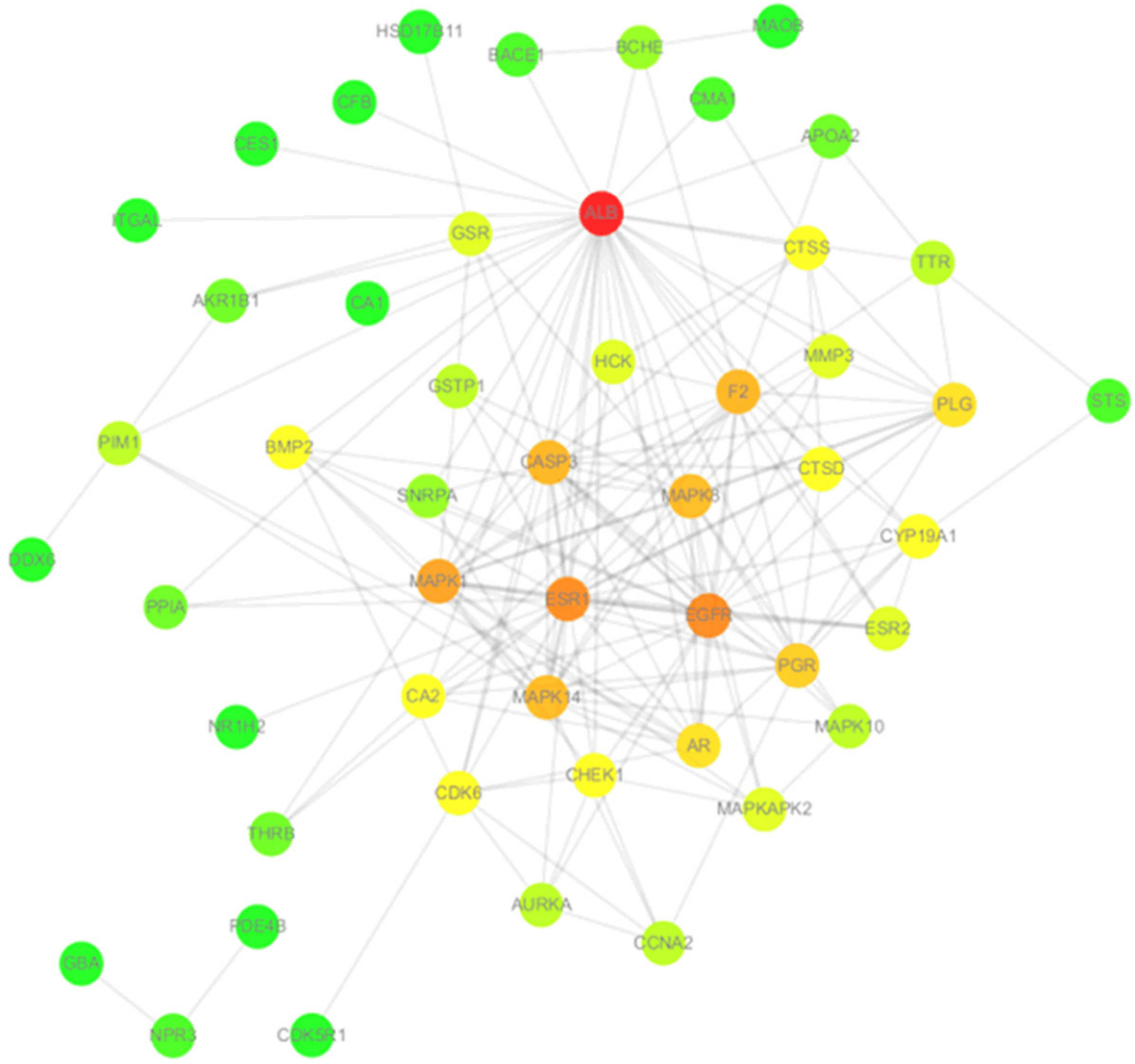

Figure 3. PPI network construction and core targets excavation. The dark nodes represented the core position in this network. The 11 core targets were excavated according to the Degree. PPI, protein-protein interaction.

Table 5. Hub genes of the PPI network with higher node degrees

Hub gene	Protein name	Node degree
ALB	Serum albumin	34
EGFR	Epidermal growth factor receptor	22
ESR1	Estrogen receptor	21
MAPK1	Mitogen-activated protein kinase 1	19
F2	Prothrombin	17
CASP3	Caspase-3	17
MAPK8	Mitogen-activated protein kinase 8	16
MAPK14	Mitogen-activated protein kinase 14	16
PGR	Progesterone receptor	14
AR	Androgen receptor	12
PLG	Plasminogen	12

we next evaluated the apoptotic ratio of these cells upon *polygonum cuspidatum* treatment. The flow cytometry results showed that the apoptotic population stained with Annexin V-FITC was dramatically increased following the treatment (**Figure 5C**). Furthermore, the immunoblotting results revealed that some of the key factors associated with MAPK and TNF signaling pathways in these cells, such as p-ERK (T202/Y204), NF-κB (p65) and IKK α/β, were significantly decreased in a dose dependent manner upon *polygonum cuspidatum* treatment, which was consistent with our previous KEGG enrichment analysis (**Figure 5D**).

Table 6. Top 10 targets of *polygonum cuspidatum* with average shortest path length and closeness centrality

Protein code	Genes	Description	Average shortest path length	Closeness centrality	R
P17342	NPR3	Atrial natriuretic peptide receptor 3	1.000000	1.000000	0.000000
P02768	ALB	Serum albumin	1.260869	0.793103	0.122449
P04062	GBA	Lysosomal acid glucosylceramidase, Lysosomal acid GCase	1.500000	0.666667	0.234694
Q07343	PDE4B	cAMP-specific 3',5'-cyclic phosphodiesterase 4B	1.500000	0.666667	0.234694
P00533	EGFR	Epidermal growth factor receptor	1.608695	0.621622	0.285714
P03372	ESR1	Estrogen receptor	1.608695	0.621622	0.285714
P28482	MAPK1	Mitogen-activated protein kinase 1, MAP kinase 1, MAPK 1	1.695652	0.589744	0.326531
P42574	CASP3	Caspase-3, CASP-3	1.695652	0.589744	0.326531
P00734	F2	Prothrombin	1.695652	0.589744	0.326531
Q16539	MAPK14	Mitogen-activated protein kinase 14, MAP kinase 14, MAPK 14	1.739130	0.575000	0.346939

Next, the levels of the aforementioned 6 core targets were determined upon *polygonum cuspidatum* treatment. The quantitative real time polymerase chain reaction (qRT-PCR) results revealed that the mRNA levels of EGFR, CASP3 and F2 were significantly downregulated by *polygonum cuspidatum* in SKOV-3 cells ($P < 0.05$; **Figure 6A**). Consistently, the protein level of EGFR was down-regulated by *polygonum cuspidatum* in a dose-dependent manner. Meanwhile, the total protein level of CASP3 was also slightly decreased, while the cleaved CASP3, a well-known apoptotic maker, accumulated significantly upon *polygonum cuspidatum* treatment (**Figure 6B**).

Systemsdock analysis of key ingredients and core targets

To further explore the action mechanism of *polygonum cuspidatum* at the protein level, we performed molecular docking analysis for its key ingredients and the corresponding core targets using SystemsDock, a unique web server that applies docking simulation for the comprehensive characterization of ligand selectivity and interpretation of ligand action on a complex molecular network [24, 25]. The docking efficiency between the UPLC-MS/MS derived 7 key ingredients (quercetin, polydatin, resveratrol, emodin, apigenin, rhein and catechin) and the 6 core targets (EGFR, CASP3, ALB, MAPK-14, F2 and ESR1) were predicted. The results showed that the overall binding affinity of polydatin with the 6 core targets (scores: 6.78, 6.58, 6.74, 6.63, 6.50 and 6.19, respectively) was greater than those of the other 6 ingredients (**Figure 7A-G**). Therefore, this result suggested that polydatin possesses a potential pharmacological activity.

Next, we further explored the druggability of polydatin using Autodock. Since our previous prediction showed that CASP3 was both a direct target of polydatin and one of the core targets of *polygonum cuspidatum*, CASP3 was selected as an example for the next docking analysis. The results showed that the physical and chemical properties of polydatin in the protein binding pocket were stable due to its rich hydroxyl groups with a good hydrophilic property. Meanwhile, the surrounding amino acids interacting with polydatin were all polar amino acids, such as Ser, Thr, Arg, Glu and Gln, which could form a strong hydrogen bond between polydatin and the protein binding pocket of CASP3 (**Figure 8**). Thus, polydatin may play a pivotal role in manifesting the therapeutic effects of *polygonum cuspidatum* via binding with CASP3. However, further experimental verification is warranted.

Discussion

Nowadays, a myriad of *in silico* target predicting methods have been used in the field of drug development [26]. In the present study, the PharmMapper database, which is based on 7,000 pharmacophore models, was utilized to search for the potential targets for the key ingredients of *polygonum cuspidatum*. The subsequent GO functional enrichment analysis of the 57 potential targets revealed a great variety of biological functions of *polygonum cuspidatum*. Furthermore, the KEGG pathway enrichment results showed that these targets were mainly involved in carcinogenesis and gyneco-

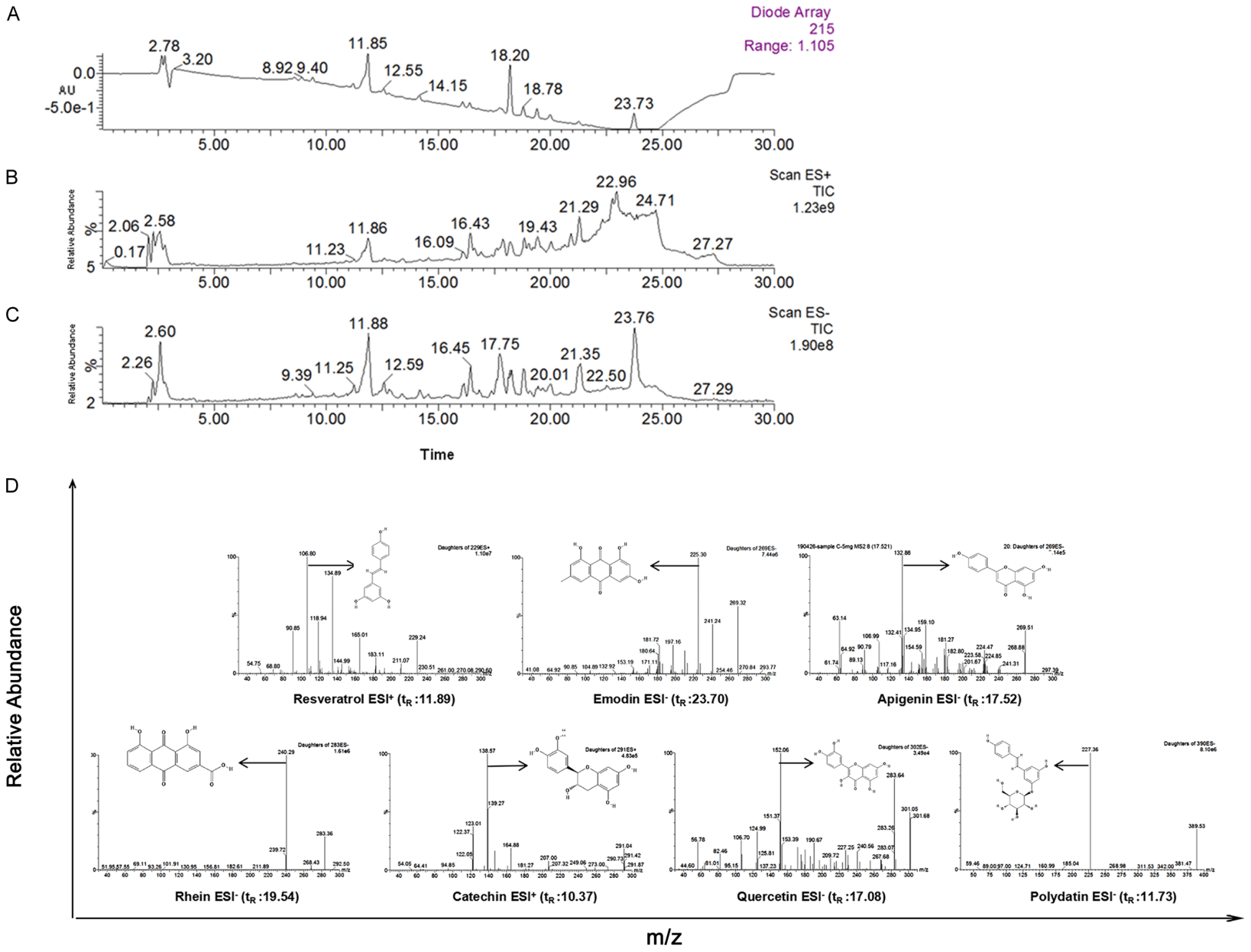
A
Diode Array
215
Range: 1.105
AU
B
Scan ES+
TIC
1.23e9
Relative Abundance
C
Scan ES-
TIC
1.90e8
Time
D
Relative Abundance
m/z
Resveratrol ESI+ (tR :11.89)
Emodin ESI- (tR :23.70)
Apigenin ESI- (tR :17.52)
Rhein ESI- (tR :19.54)
Catechin ESI+ (tR :10.37)
Quercetin ESI- (tR :17.08)
Polydatin ESI- (tR :11.73)

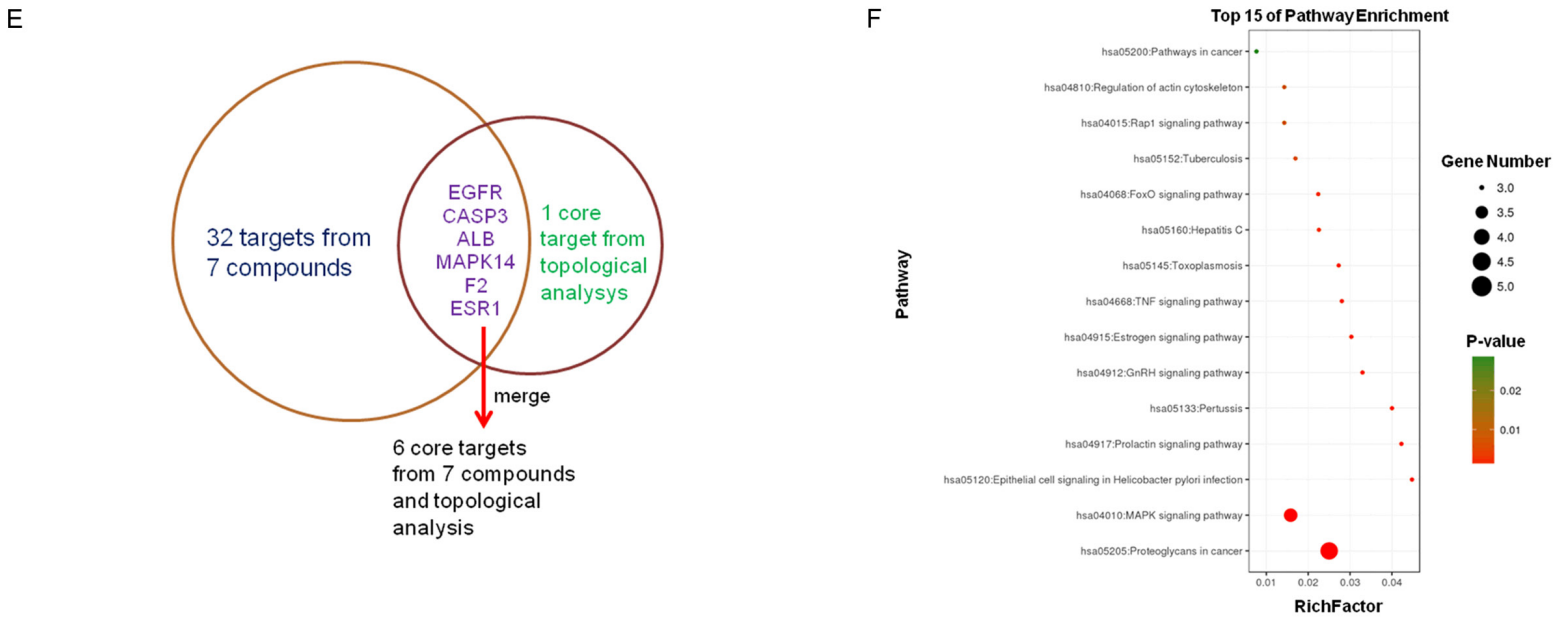

Figure 4. Seven main ingredients obtained from the crude extract of *polygonum cuspidatum* by using the UPLC-MS/MS method. A. Ultraviolet absorption wavelength map. B. Total Ion Chromatography (TICs) in positive ion modes. C. Total Ion Chromatography (TICs) in negative ion modes. D. Identification maps of the 7 main ingredients by secondary mass spectrometry. E. Venn diagram (6 core targets from 7 main ingredients and topological analysis). F. KEGG enrichment analysis map of 6 core targets by DAVID Bioinformatics Resources 6.8. The size of the dots indicated the number of enriched genes, and the color of the dots represented the degree of significance based on the *p*-value.

Table 7. Identification of compounds in *Polygonum cuspidatum* by UPLC-MS data

No.	t_R (min)	Molecular formula	Selected ion	Theoretical	Experimental	MS/MS fragmentions	Compounds
1	11.89	$C_{14}H_{12}O_3$	$[M+H]^+$	228.24	229.24	211.07, 183.11, 165.01, 134.89, 118.94, 106.80, 90.85	Resveratrol
2	23.70	$C_{15}H_{10}O_5$	$[M-H]^-$	270.24	269.32	241.24, 225.30, 181.72	Emodin
3	17.52	$C_{15}H_{10}O_5$	$[M-H]^-$	270.24	269.51	159.10, 132.86, 106.99, 63.14	Apigenin
4	19.54	$C_{15}H_8O_6$	$[M-H]^-$	284.22	283.36	240.29	Rhein
5	10.37	$C_{15}H_{14}O_6$	$[M+H]^+$	290.27	291.04	138.57, 123.01	Catechin
6	17.08	$C_{15}H_{10}O_7$	$[M-H]^-$	302.24	301.05	283.64, 152.06, 124.99, 106.70, 82.46	Quercetin
7	11.73	$C_{20}H_{22}O_8$	$[M-H]^-$	390.39	389.53	227.36	Polydatin

logical diseases. Indeed, accumulating evidence have shown that *polygonum cuspidatum* and its active ingredients exhibit anti-cancer effects either through direct inhibition of cancer cell growth or through the modulation of the host immune-system [27-31]. In addition, recent pharmacological studies showed that *polygonum cuspidatum* extractor its major ingredients possessed anti-virus and anti-inflammatory activities, which may, at least partially, reflect the therapeutic effects of *polygonum cuspidatum* on those cancerous and gynecological diseases attributed to viral infection or inflammation [32-35]. Of note, different active ingredients of *polygonum cuspidatum*, such as resveratrol and polydatin, may exert their therapeutic functions via distinct mechanisms. For instance, polydatin could inhibit cell growth and induce the apoptosis of HCC cells by blocking the STAT3 signaling pathway, while resveratrol inhibiting the epithelial mesenchymal transition through inactivation of the PI-3K/Akt/NF-κB and hedgehog signaling pathways [36-39]. Therefore, the present action mechanism study guided by network pharmacology may help provide a deeper insight into the "multi-component, multi-target and multi-function" characteristics of *polygonum cuspidatum* in cancerous and gynecological diseases.

To untangle the complicated interactions among the potential targets of the key ingredients in *polygonum cuspidatum*, a PPI network was constructed based on a key topological parameter, degree, using STRING and Cytoscape 3.2.1. Eleven core targets were found to have higher degrees of connectivity within this network. Besides the degree, other topological parameters, such as shortest path length and closeness centrality, could also be used for assessing the importance of key nodes (core targets) within a network. The nodes with a small average shortest path length and a large closeness centrality (R-value) were usually considered as the important targets in the network [40]. We therefore developed a novel formula, in which the "R value" is determined by the average shortest path length and closeness centrality, to validate the reliability of the above 11 predicted core targets. Notably, among the top 10 core targets (ranked based on R-values) excavated using this new formula, 7 overlapped with the former 11 core targets, showing a good consistency among the different prediction algorithms.

Noteworthy, 7 ingredients of *polygonum cuspidatum* were validated by UPLC-MS/MS, among the 14 putative ones derived from the network pharmacological prediction. Of these 7 ingredients, only 3 met the medicinal criteria for the selection of active ingredients (OB ≥ 30% and DL ≥ 0.18), indicating the importance of literature mining to the selection of active ingredients by network pharmacology. Interestingly, 6 potential targets derived from these 7 ingredients overlapped with the 7 core targets excavated from the previous PPI network analyses, underscoring the pivotal role of these 6 targets in the action mechanism of *polygonum cuspidatum*. Our further molecular docking analysis between these 6 targets and 7 ingredients showed that polydatin possesses a better pharmacological activity, as compared to the other 6 ingredients, implying a leading role of polydatin in delivering the therapeutic effects of *polygonum cuspidatum*. Indeed, among the 6 aforementioned potential targets of *polygonum cuspidatum*, EGFR and CASP3 have previously been identified as the putative targets of polydatin using PharmMapper and ChemMapper algorithms (7). In the present study, we confirmed that EGFR and CASP3 were down-regulated at both mRNA and protein levels by qRT-

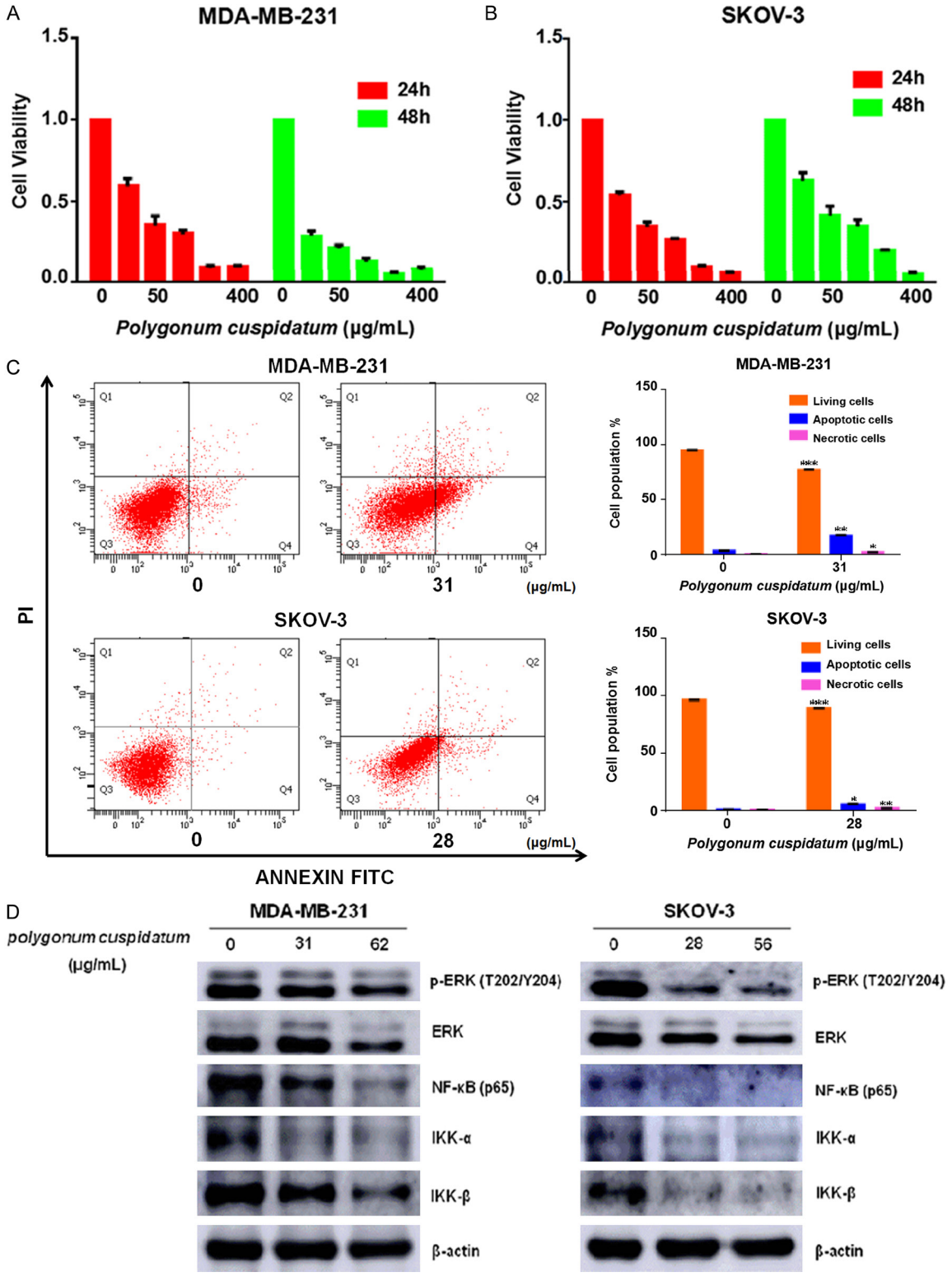

Figure 5. *Polygonum cuspidatum* decreased the viability and induced apoptosis of MDA-MB-231 and SKOV-3 cells. A, B. CCK-8 assay was performed to measure cell proliferation rate at 24 and 48 h after *polygonum cuspidatum* treatment at different dosages (0, 25, 50, 100, 200 and 400 μg/ml). C. Induction of apoptosis of MDA-MB-231 and SKOV-3 cells after *polygonum cuspidatum* treatment. MDA-MB-231 cells were treated with *polygonum cuspidatum* at different concentrations (0 and 31 μg/ml) for 24 h, and SKOV-3 cells were also treated with *polygonum cuspidatum* at different concentrations (0 and 28 μg/ml) for 24 h, when apoptotic events were assessed by flow cytometry. Statistical analysis of the percentage of apoptosis in MDA-MB-231 and SKOV-3 cells $^{**}P < 0.01$ based on Student's

t-test. D. MDA-MB-231 and SKOV-3 cells were treated with *polygonum cuspidatum* at different concentrations (0, 31, 62 μg/ml or 0, 28, 56 μg/ml) for 24 h. After proteins were extracted, the protein levels of p-ERK (T202/Y204), ERK, NF-κB, IKK-α and IKK-β were analyzed by western blot.

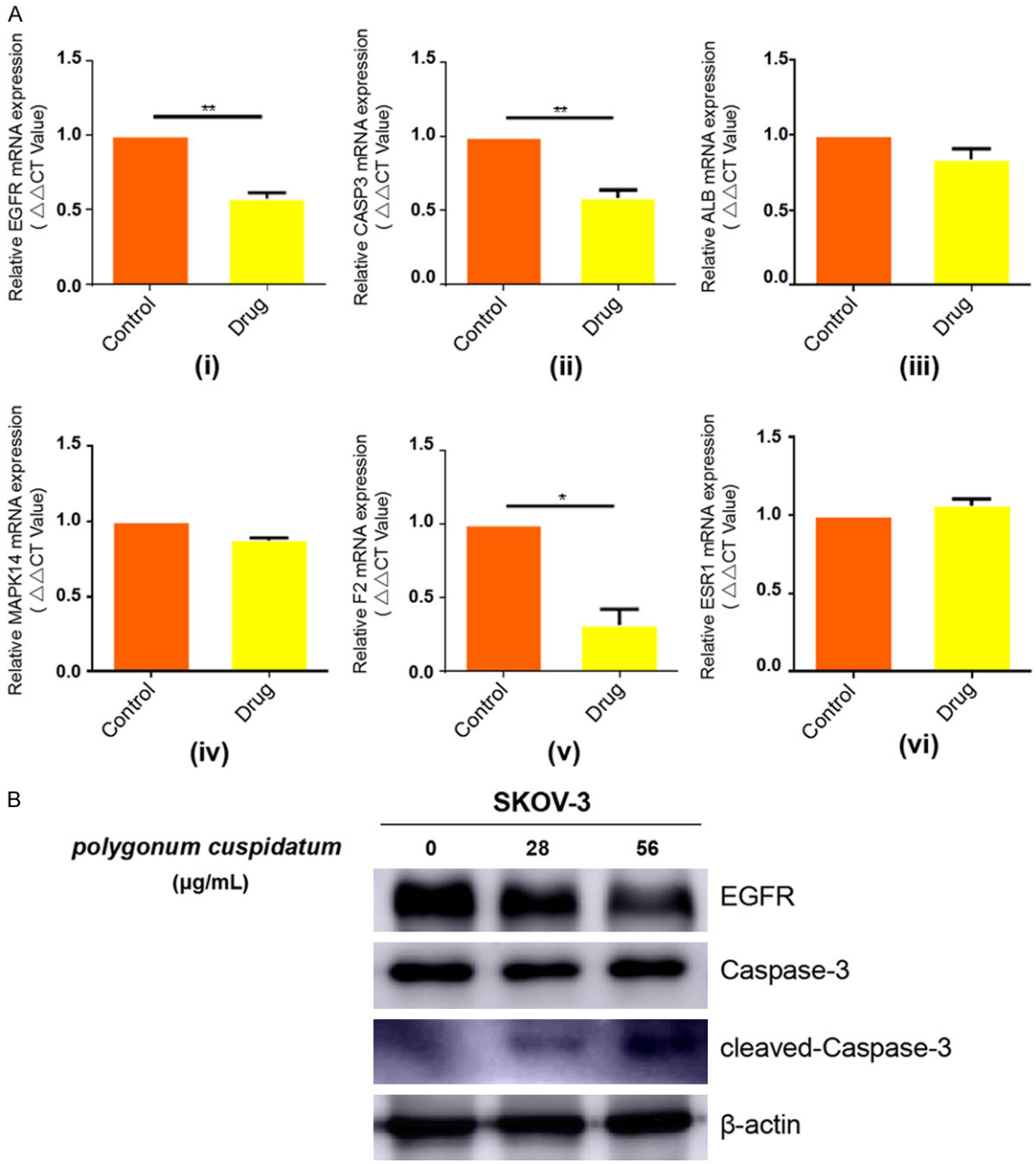

Figure 6. The mRNA and protein expression levels of six core targets. A. The mRNA expression levels of 6 core targets were analyzed by qRT-PCR in human ovarian cancer SKOV-3 cells. **P < 0.01 based on Student's *t*-test. qRT-PCR, quantitative real time polymerase chain reaction. B. SKOV-3 cells were treated with *polygonum cuspidatum* at different concentrations (0, 28, 56 μg/ml) for 24 h. After proteins were extracted, the protein levels of EGFR and CASP3 were analyzed by western blot.

PCR and western blot in *polygonum cuspidatum*-treated cells, accompany with the accumulation of the cleaved CASP3, which was in line with the apoptotic phenotype induced by polydatin in this and other studies [36, 41]. These results further suggested that polydatin could

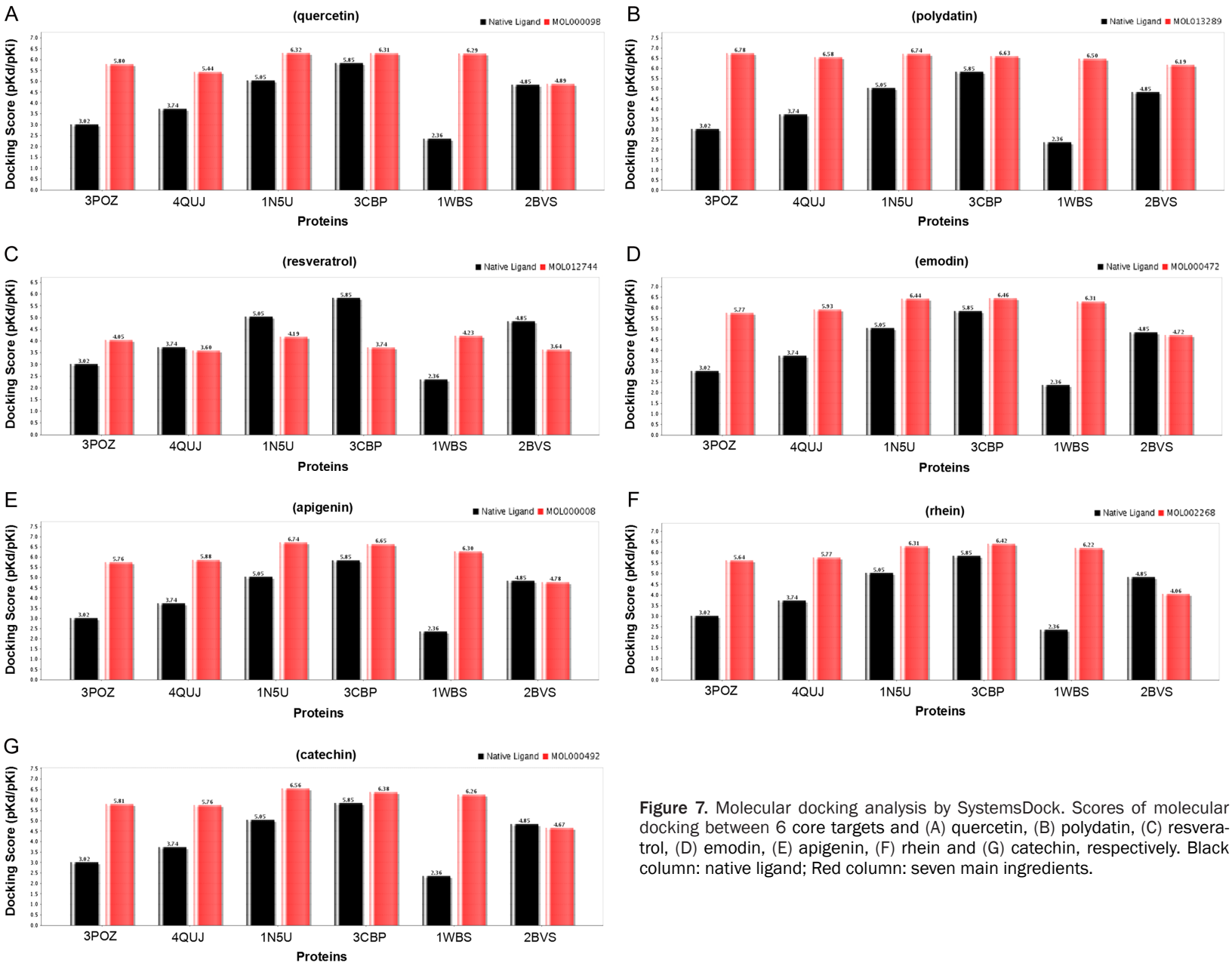

Figure 7. Molecular docking analysis by SystemsDock. Scores of molecular docking between 6 core targets and (A) quercetin, (B) polydatin, (C) resveratrol, (D) emodin, (E) apigenin, (F) rhein and (G) catechin, respectively. Black column: native ligand; Red column: seven main ingredients.

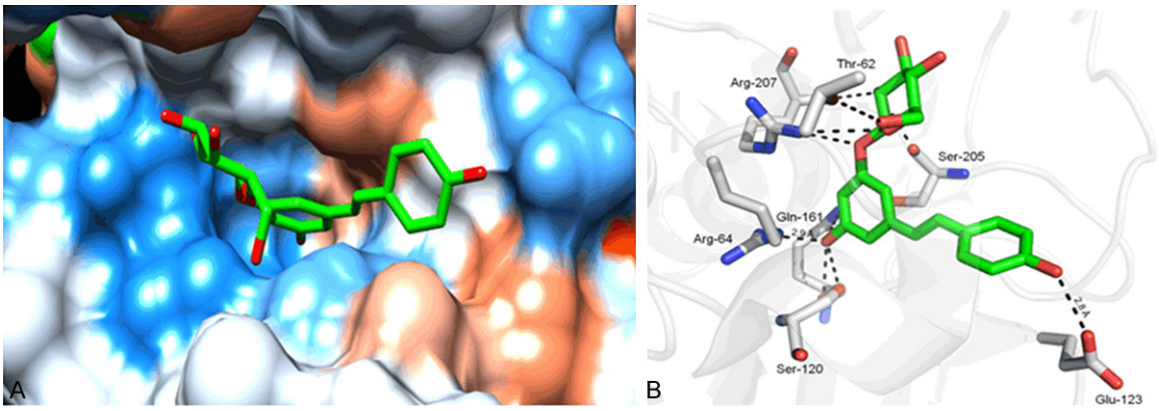

Figure 8. Binding modes from Autodock. Hydrophilic-hydrophobic interaction between (A) Polydatin and CASP3 in protein binding pocket, and (B) Polydatin and relative amino acids. CASP3, caspase-3.

exert its inhibitory effects on these two targets at both mRNA and protein levels. Nevertheless, polydatin exhibited its antiproliferation effect on different cancerous cells via distinct mechanisms. For instance, polydatin could arrest the leukemia cells in the S-phase by inhibiting the expression of cyclins D1 and B1, while inhibiting the proliferation of breast cancer cells by inactivating Creb [42, 43]. Therefore, the detailed action mechanism of polydatin underlying its therapeutic effect on specific cell types warrants further investigation.

Acknowledgements

This study was funded by the National Natural Science Foundation of China (grant no. 815-72416), the National Key Technologies R & D Program of China (grant no. 2016YFC1303200) and the Tianjin Medical University Cancer Institute & Hospital Cancer Translational Medicine Seed Funds (grant no. 1701-1).

Disclosure of conflict of interest

None.

Abbreviations

CHM, Chinese herb medicine; PPI, protein-protein interaction; OB, oral bioavailability; DL, drug-likeness; EGFR, epidermal growth factor receptor; CASP3, caspase-3; TICs, Total Ion Chromatography.

Address correspondence to: Liren Liu, Department of Gastrointestinal Cancer Biology, National Clinical Research Center of Cancer, Tianjin Medical University Cancer Institute and Hospital, Huanhuxi Road, Tianjin 300060, China. E-mail: liuliren@tmu.edu.cn

References

[1] Gao H, Wang Z, Li Y and Qian Z. Overview of the quality standard research of traditional Chinese. Front Med 2011; 5: 195-202.

[2] Tang WM, Chan E, Kwok CY, Lee YK, Wu JH, Wan CW, Chan RY, Yu PH and Chan SW. A review of the anticancer and immunomodulatory effects of *lyciumbarbarum* fruit. *Inflammopharmacology* 2011; 20: 307-14.

[3] Chan SW. Panax ginseng, *rhodiolarosea* and *schisandra chinensis*. *Int J Food Sci Nutr* 2012; 2012: 75-81.

[4] Peng W, Qin R, Li X and Zhou H. Botany, phytochemistry, pharmacology, and potential application of polygonum cuspidatum Sieb.et Zucc.: a review. J Ethnopharmacol 2013; 148: 729-45.

[5] Matsuda H, Shimoda H, Morikawa T and Yoshikawa M. Phytoestrogens from the roots of polygonum cuspidatum (polygonaceae): structure-requirement of hydroxyanthraquinones for estrogenic activity. Bioorg Med Chem Lett 2001; 11: 1839-42.

[6] Liu H, Zhan S, Zhang Y, Ma Y, Chen L, Chen L, Dong H, Ma M and Zhang Z. Molecular network-based analysis of the mechanism of liver injury induced by volatile oils from Artemisiaeargyi folium. BMC Complement Alteru Med 2017; 17: 491.

[7] Pan BY, Ren YY and Liu LR. Uncovering the action mechanism of polydatin via network pharmacological target prediction. RSC Adv 2018; 8: 18851.

[8] Hong M, Li S, Tan HY, Cheung F, Wang N, Huang J and Feng Y. A network-based pharmacology study of the herb-induced liver injury potential of traditional hepatoprotective Chinese herbal medicines. Molecules 2017; 22: 632-46.

[9] Lyu M, Yan CL, Liu HX, Wang TY, Shi XH, Liu JP, Orgah J, Fan GW, Han JH, Wang XY and Zhu Y. Network pharmacology exploration reveals en-

dothelial inflammation as a common mechanism for stroke and coronary artery disease treatment of Danhong injection. Sci Rep 2017; 7: 15427-45.
[10] Zhang A, Fang H, Wang Y, Yan G, Sun H, Zhou X, Wang Y, Liu L and Wang X. Discovery and verification of the potential targets from bioactive molecules by network pharmacology-based target prediction combined with high-throughput metabolomics. RSC Adv 2017; 7: 51069-78.
[11] Hong M, Zhang Y, Li S, Tan HY, Wang N, Mu S, Hao X and Feng Y. A network pharmacology-based study on the hepatoprotective effect of fructus schisandrae. Molecules 2016; 22: 1617-28.
[12] Pei T, Zheng C, Huang C, Chen X, Guo Z, Fu Y, Liu J and Wang Y. Systematic understanding the mechanisms of vitiligo pathogenesis and its treatment by qubaibabuqi formula. J Ethnopharmacol 2016; 190: 272-87.
[13] Zhang W, Tao Q, Guo Z, Fu Y, Chen X, Shar PA, Shahen M, Zhu J, Xue J, Bai Y, Wu Z, Wang Z, Xiao W and Wang Y. Systems pharmacology dissection of the integrated treatment for cardiovascular and gastrointestinal disorders by traditional Chinese medicine. Sci Rep 2016; 6: 32400.
[14] Li B, Weng Q, Dong C, Zhang Z, Li R, Liu J, Jiang A, Li Q, Jia C, Wu W and Liu H. A key gene, PLIN1, can affect porcine intramuscular fat content based on transcriptome analysis. Genes 2003; 9: 194.
[15] de Jong H, Geiselmann J, Hernandez C and Page M. Genetic network analyzer: qualitative simulation of genetic regulatory networks. Bioinformatics 2003; 19: 336-44.
[16] Ru J, Li P, Wang J, Zhou W, Li B, Huang C, Li P, Guo Z, Tao W, Yang Y, Xu X, Li Y, Wang Y and Yang L. Tcmsp: a database of systems pharmacology for drug discovery from herb medicines. J Cheminf 2014; 6: 13.
[17] Shi S, Pan M and Wang W. Research progress on chemical in roots and rhizomes of polygonum cuspidatum and their pharmacological activities. Drug Evaluation Research (Chinese Journal) 2016; 39: 317-21.
[18] Kong X and Zhou L. Study progress of giant knotweed rhizome. Guiding Journal of Traditional Chinese Medicine and Pharmacy (Chinese Journal) 2009; 15: 107-10.
[19] Chen S, Tao J, Zhong F, Jiao Y, Xu J, Shen Q, Wang H, Fan S and Zhang Y. Polydatin down-regulates the phosphorylation level of Creb and induces apoptosis in human breast cancer cell. PLoS One 2017; 12: e0176501.
[20] Li H, Shi B, Li Y and Yin F. Polydatin inhibits cell proliferation and induces apoptosis in laryngeal cancer and HeLa cells via suppression of the PDGF/AKT signaling pathway. Biochem Mol Toxicol 2017; 31: e21900.
[21] Díaz-Chávez J, Fonseca-Sánchez MA, Arechaga-Ocampo E, Flores-Pérez A, Palacios-Rodríguez Y, Domínguez-Gómez G, Marchat LA, Fuentes-Mera L, Mendoza-Hernández G, Gariglio P and López-Camarillo C. Proteomic profiling reveals that resveratrol inhibits HSP27 expression and sensitizes breast cancer cells to doxorubicin therapy. PLoS One 2013; 8: e64378.
[22] Park SH, Seong MA and Lee HY. p38 MAPK-induced MDM2 degradation confers paclitaxel resistance through p53-mediated regulation of EGFR in human lung cancer cells. Oncotarget 2016; 7: 8184-99.
[23] O'Leary KA, Jallow F, Rugowski DE, Sullivan R, Sinkevicius KW, Greene GL and Schuler LA. Prolactin activates ERα in the absence of ligand in female mammary development and carcinogenesis in vivo. Endocrinology 2013; 154: 4483-92.
[24] Hsin KY, Matsuoka Y, Asai Y, Kamiyoshi K, Watanabe T, Kawaoka Y and Kitano H. Systemsdock a web server for network pharmacology-based prediction and analysis. Nucleic Acids Res 2016; 44: W507-13.
[25] Hsin KY, Ghosh S and Kitano H. Combining machine learning systems and multiple docking simulation packages to improve docking prediction reliability for network pharmacology. PLoS One 2013; 8: e83922.
[26] Cereto-Massagué A, Ojeda MJ, Valls C, Mulero M, Pujadas G and Garcia-Vallve S. Tools for in silico target fishing. Methods 2015; 71: 98-103.
[27] Wu X, Li Q, Feng Y and Ji Q. Antitumor research of the active ingredients from traditional Chinese medical plant polygonum cuspidatum. Evid Based Complement Alternat Med 2018; 2018: 2313021.
[28] Li W, Zhang Q, Chen K, Sima Z, Liu J, Yu Q and Liu J. 2-Ethoxystypandrone, a novel small-molecule STAT3 signaling inhibitor from polygonum cuspidatum, inhibits cell growth and induces apoptosis of HCC cells and HCC Cancer stem cells. BMC Complement Altern Med 2019; 19: 38.
[29] Wang YL, Horng CT, Hsieh MT, Chen HC, Huang YS, Yang JS, Wang GK, Chiang JH, Chen HH, Lu CC and Chen FA. Autophagy and apoptotic machinery caused by polygonum cuspidatum extract in cisplatin resistant human oral cancer CAR cells. Oncol Rep 2019; 41: 2549-57.
[30] Chueh FS, Lin JJ, Lin JH, Weng SW, Huang YP and Chung JG. Crude extract of polygonum cuspidatum stimulates immune responses in normal mice by increasing the percentage of Mac-3-positive cells and enhancing macro-

phage phagocytic activity and natural killer cell cytotoxicity. Mol Med Rep 2015; 11: 127-32.
[31] Chueh FS, Lin JJ, Lin JP, Yu FS, Lin JH, Ma YS, Huang YP, Lien JC and Chung JG. Crude extract of Polygonum cuspidatum promotes immune responses in leukemic mice through enhancing phagocytosis of macrophage and natural killer cell activities in vivo. In Vivo 2015; 29: 255-61.
[32] Chang JS, Liu HW, Wang KC, Chen MC, Chiang LC, Hua YC and Lin CC. Ethanol extract of polygonum cuspidatum inhibits hepatitis B virus in a stable HBV-producing cell line. Antivir Res 2005; 66: 29-34.
[33] Lin HW, Sun MX, Wang YH, Yang LM, Yang YR, Huang N, Xuan LJ, Xu YM, Bai DL, Zheng YT and Xiao K. Anti-HIV activities of the compounds isolated from polygonum cuspidatum and polygonum multiflorum. Planta Med 2010; 76: 889-92.
[34] Wang QW, Su Y, Sheng JT, Gu LM, Zhao Y, Chen XX, Chen C, Li WZ, Li KS and Dai JP. Anti-influenza a virus activity of rhein through regulating oxidative stress, TLR4, Akt, MAPK, and NF-κB signal pathways. PLoS One 2018; 13: e0191793.
[35] Han JH, Koh W, Lee HJ, Lee HJ, Lee EO, Lee SJ, Khil JH, Kim JT, Jeong SJ and Kim SH. Analgesic and anti-inflammatory effects of ethyl acetate fraction of polygonum cuspidatum in experimental animals. Immunopharm Immunot 2012; 34: 191-5.
[36] Jiao Y, Wu Y and Du D. Polydatin inhibits cell proliferation, invasion and migration, and induces cell apoptosis in hepatocellular carcinoma. Braz J Med Biol Res 2018; 51: e6867.
[37] Li W, Ma J, Ma Q, Li B, Han L, Liu J, Xu Q, Duan W, Yu S, Wang F and Wu E. Resveratrol inhibits the epithelial-mesenchymal transition of pancreatic cancer cells via suppression of the PI-3K/Akt/NF-κB pathway. Curr Med Chem 2013; 20: 4185-94.
[38] Wang H, Zhang H, Tang L, Chen H, Wu C, Zhao M, Yang Y, Chen X and Liu G. Resveratrol inhibits its TGF-β1-induced epithelial-to-mesenchymal transition and suppresses lung cancer invasion and metastasis. Toxicology 2013; 303: 139-46.
[39] Li J, Chong T, Wang Z, Chen H, Li H, Cao J, Zhang P and Li H. A novel anti-cancer effect of resveratrol: reversal of epithelial-mesenchymal transition in prostate cancer cells. Mol Med Rep 2014; 10: 1717-24.
[40] Anitha P, Anbarasu A and Ramaiah S. Gene network analysis reveals the association of important functional partners involved in antibiotic resistance: a report on an important pathogenic bacterium staphylococcus aureus. Gene 2016; 575: 253-63.
[41] Liu H, Zhao S, Zhang Y, Wu J, Peng H, Fan J and Liao J. Reactive oxygen species-mediated endoplasmic reticulum stress and mitochondrial dysfunction contribute to polydatin-induced apoptosis in human nasopharyngeal carcinoma CNE cells. J Cell Biochem 2011; 112: 3695-703.
[42] Cao WJ, Wu K, Wang C and Wan DM. Polydatin-induced cell apoptosis and cell cycle arrest are potentiated by Janus kinase 2 inhibition in leukemia cells. Mol Med Rep 2016; 13: 3297-302.
[43] Chen S, Tao J, Zhong F, Jiao Y, Xu J, Shen Q, Wang H, Fan S and Zhang Y. Polydatin down-regulates the phosphorylation level of Creb and induces apoptosis in human breast cancer cell. PLoS One 2017; 12: e0176501.